ACS APPLIED POLYMER MATERIALS

Open Access

This article is licensed under CC-BY 4.0

pubs.acs.org/acsapm

Article

Force-Induced Structural Changes in Spider Silk Fibers Introduced by ATR-FTIR Spectroscopy

Mohammad Javad Jafari, Fredrik G. Bäcklund, Tina Arndt, Benjamin Schmuck, Gabriele Greco, Anna Rising, Andreas Barth, and Thomas Ederth*

Cite This: ACS Appl. Polym. Mater. 2023, 5, 9433−9444

Read Online

ACCESS | Metrics & More | Article Recommendations | Supporting Information

ABSTRACT: Silk fibers have unique mechanical properties, and many studies of silk aim at understanding how these properties are related to secondary structure content, which often is determined by infrared spectroscopy. We report significant method-induced irreversible structural changes to both natural and synthetic spider silk fibers, derived from the widely used attenuated total reflection Fourier-transform infrared (ATR-FTIR) technique. By varying the force used to bring fibers into contact with the internal reflection elements of ATR-FTIR accessories, we observed correlated and largely irreversible changes in the secondary structure, with shape relaxation under pressure occurring within minutes. Fitting of spectral components shows that these changes agree with transformations from the α-helix to the β-sheet secondary structure with possible contributions from other secondary structure elements. We further confirm the findings with IR microspectroscopy, where similar differences were seen between the pressed and unaffected regions of spider silk fibers. Our findings show that ATR-FTIR spectroscopy requires care in its use and in the interpretation of the results.

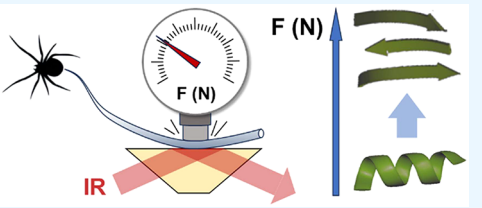

KEYWORDS: *silk fibers, ATR-FTIR, secondary structure, pressure effects, spider silk, NT2RepCT minispidroin*

INTRODUCTION

Silk fibers from moths and the various types of silk fibers spun by spiders exhibit remarkable mechanical properties; in particular, the major ampullate silk displays extraordinarily high toughness.[1−4] To understand how structure and properties are related in silk and silk-like fibers, it is essential to clarify their structural composition. Infrared spectroscopic methods are well established and widely used for investigating the secondary structure of proteins and protein constructs,[5−7] also including silk.[8−10] A sampling method that has been used in numerous studies of silk fibers is ATR-FTIR.[9,11−13] In ATR, infrared light undergoes total internal reflection at the surface of an IR-transparent prism (the internal reflection element, IRE) to create an evanescent wave at the prism surface onto which the sample is positioned. The evanescent wave probes a depth of the order of a few micrometers into the sample, and the technique requires the sample to be in close contact with the prism of the ATR device. For solids, gels, and other nonfluidic samples, this is accomplished by pressing the sample toward the prism with a piston or plunger, which is normally an integrated part of the ATR accessory and which typically has some force-limiting mechanism which serves to avoid excessive pressure on the IRE and to improve repeatability by minimizing the spread in applied pressure between measurements. Although this technique has been used in many previous studies on fibrous structures, including protein-based fibers,[14−18] it has potential drawbacks when investigating samples where the microstructure is sensitive to external pressure.

Several studies demonstrate pressure effects on silk fibers, for example, effects of hydrostatic pressure and uniaxial stress on major ampullate spider silk fibers,[19] changes in amorphous and nanocrystalline phases of major ampullate spider silk under pressure,[20] and combined effects of pressure and hydration on spider[21] and silkworm[22] silk films, respectively. Some of these studies[21,22] used ATR-FTIR to monitor the pressure effects, though these studies were not made *in situ*; that is, the pressure was not applied with the ATR-FTIR sampling accessory, but by subjecting the fibers to isotropic hydrostatic pressure, which could affect the fibers in different ways compared to the highly directed pressure used for ATR-FTIR sampling and where the latter is more likely to induce plastic deformation.

Differences between IR spectra recorded using different techniques, such as the transmission mode, diffuse reflectance, or ATR, have been described in the literature[23,24] and can be largely explained by effects specific to the different sampling techniques, for example, the anomalous dispersion effect,[25,26] and are routinely handled with correction procedures for

Received: August 16, 2023
Revised: October 9, 2023
Accepted: October 9, 2023
Published: October 30, 2023

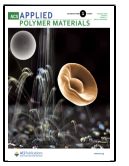

Downloaded via SWEDISH UNIV AGRICULTURAL SCIENCES on December 5, 2023 at 07:30:54 (UTC).
See https://pubs.acs.org/sharingguidelines for options on how to legitimately share published articles.

© 2023 The Authors. Published by American Chemical Society

making spectra comparable. Beyond these corrections, there might be differences remaining between techniques due to the treatment of the samples in preparation for the specific sampling methods. For example, the use of ATR-FTIR for silk fibers from silkworms and spiders has previously been compared with alternative methods for generating FTIR structural data. It was then postulated that microstructural modifications might be introduced due to the inevitable pressure put on the sample when using ATR-FTIR.[24] However, in the study by van Nimmen at al.,[24] the differences in the resulting FTIR spectra obtained with different sampling techniques were not conclusively linked to structural deformations originating with the ATR-FTIR setup, and the interpretation is obscured by irregularities in the spectra obtained with the other sampling techniques. On the other hand, there are also examples in the literature where ATR-FTIR has produced results in agreement with other techniques, such as recent work by Carissimi et al.[12] on the secondary structure of silkworm fibroin nanoparticles, where ATR-FTIR and nuclear magnetic resonance (NMR) spectroscopy produced consistent results.

A more recently developed alternative to ATR-FTIR is that of IR microspectroscopy,[27] offering the possibility of measurements in both transmission and reflection modes. For either of these, issues arising specifically from bringing the sample in close contact with a substrate, such as those needed for ATR measurements, can be avoided, if the sample can be securely held in place. IR microspectroscopy in reflectance mode has previously been considered primarily suitable for flat surfaces.[28] However, IR microspectroscopy, and also Raman microspectroscopic techniques, have been used successfully on moth and spider silk fibers.[29,30] Furthermore, as shown in a study comparing ATR-FTIR and reflectance mode IR microspectroscopy for the classification of a range of textile fiber types, the latter represents a viable alternative to ATR-FTIR.[31] In this study, conventional ATR-FTIR spectroscopy was found to deform the sample, although for the materials investigated this was not deemed to significantly alter the spectra. Deformation may have small effects on the IR spectra of sturdy fiber types, but the pressure applied to structurally more malleable fibers during ATR-FTIR spectroscopy could induce deformations, which significantly affect the obtained results. This was tentatively concluded in a recent study conducted on historical silk samples.[32] Although there is ample evidence that the ATR-FTIR technique potentially induces changes in the structure of silk samples, which could complicate or preclude structural interpretation of the data, it appears that this aspect has not been systematically investigated.

Here, we make a quantitative assessment of the effect of the applied force during ATR-FTIR measurements on spider silk fibers. With a load cell attached to the pressing device of an ATR accessory, we monitor the applied force on the fibers during the measurements and correlate this to the observed changes in secondary structure, as obtained by fitting of spectral components to the observed amide bands. By comparing results obtained from natural and synthetic spider silk fibers in contact with the internal reflection elements of ATR-FTIR sampling accessories under different applied loads, we demonstrate that regular ATR-FTIR sampling can induce structural changes that considerably affect the interpretation of the results in terms of chain conformation and the secondary structure. Evaluating the spectra before and after applying the loads and under controlled applied forces, we find that already at low forces the effects on the resulting spectra are permanent. Rather than applying hydrostatic pressure to the fibers, which acts isotropically and which has been used in previous studies of pressure-induced effects on silk,[19−21] we use a piston to press fibers directly onto the ATR prisms because this is necessary to bring the sample in sufficiently close contact with the internal reflection element for probing the sample, and it is also the normal procedure for ATR sampling, which is the measurement situation under scrutiny.

MATERIALS AND METHODS

Preparation of Artificial Spider Silk Fibers. Protein expression and purification of the minispidroin NT2RepCT[33] was performed in native conditions as described earlier.[34] After purification, the spinning dope was prepared by concentrating NT2RepCT stored in a 20 mM Tris-HCl buffer at pH 8 to 300 mg/mL using a centrifugal filter with a 10 kDa cutoff (Amicon Ultra-15 equipped with a Ultracel-10K filter) at 4 °C and 4000*g*. Then, artificial spider silk fibers were made according to a recently described spinning protocol that was optimized for NT2RepCT.[35] The spinning dope was extruded at a rate of 17 μL/min via a pulled glass capillary having an orifice diameter of 55 ± 5 μm into a spinning bath containing a 0.75 M acetate buffer at pH 5. In the spinning bath, extruded NT2RepCT instantaneously formed a solid fiber, which was collected at the end of the 80 cm long spinning bath at a collection speed of 58 cm/s. The temperature and humidity during spinning and fiber collection were 22 °C and 30 ± 10%, respectively. No postspin stretching was applied. From microscopy images, the diameter of the used NT2RepCT fibers was estimated to approximately 16 μm.

Collection of Major Ampullate Spider Silk Fibers. Major ampullate spider silk fibers from the species *Larinioides sclopetarius* were extracted at ca. 1 cm/s by stimulating the spinnerets of a fixed spider under a stereomicroscope (Leica M60). From microscopy images the diameter of the fibers was estimated to approximately 5 μm.

Infrared Spectroscopy. For regular (nonimaging) ATR-FTIR, a PIKE MIRacle accessory (PIKE Technologies, Madison, WI) was used in a Bruker Vertex 70 spectrometer, with a DLaTGS detector, at 2 cm^{-1} resolution, adding 64 scans for each spectrum. The accessory was used with a single-reflection diamond-coated ZnSe crystal (IRE), with a circular 1.8 mm diameter surface for the sample. The sample clamp has a torque-limiting mechanism set to apply a maximum force of ca. 180 N. For consistent results (best repeatability), it is recommended that the pressure on the sample is increased with the clamp until the torque-limiting mechanism is triggered, i.e., when maximum applied load is reached. Fifteen fibers were taped to a frame which was placed across the prism for each measurement, but with some fibers breaking in the preparation process, about 10−12 were typically remaining during the measurements. For the polarized measurements, the fibers were placed on the prism in a direction parallel to the IR beam (though tests comparing the perpendicular orientation of the fibers did not show any significant differences between the two orientations). ATR spectra under increasing loads obtained under different polarizations (and nonpolarized light) were acquired in separate series for each polarization direction to maintain stable measurement conditions. For each series, a background spectrum and the subsequent measurements under increasing load were performed with the polarizer fixed. The measurements under different polarizations were performed on the same fiber bundle but translating the bundle over the IRE between the measurements to probe a pristine region of the fibers at the start of each measurement.

Imaging ATR-FTIR was performed with an Imaging Golden Gate accessory (Specac, UK) with ZnSe optics in a Bruker IMAC macrochamber with a 128 × 128 pixel focal plane array detector. A Bruker Tensor 27 spectrometer was used as a light source, with 2 cm^{-1} resolution, and 32 scans were added for each image. The sample

https://doi.org/10.1021/acsapm.3c01892
ACS Appl. Polym. Mater. 2023, 5, 9433−9444

surface is a 2 × 2 mm^2 diamond prism, and the sample can be pressed to this surface with forces up to 800 N using the provided clamp.

All ATR spectra were corrected for the wavelength-dependent penetration depth into the ATR IRE, but not for the anomalous dispersion effect in regions of strong absorbance.

For IR microspectroscopy, a Bruker Hyperion 3000 IR microscope was used in reflection mode. A Bruker Tensor 27 spectrometer was used as a light source at 4 cm^{-1} resolution, accumulating 100 scans for each image. A 15× reflective (Cassegrain) objective was used for imaging, and a 128 × 128 pixel focal plane array was used as the detector. Samples were mounted on gold-coated glass slides to provide a reflective background.

Load Control. A custom-made load cell adapter for monitoring of the applied force during ATR measurements, based on a 500 N load cell (TE Connectivity FX29, model FX293X-100A-0100-L), was used to measure the force applied to the fibers under the controlled load experiments (Figure S1 in the Supporting Information), with both ATR accessories. Calibration of the load cell is described in Figure S2. The load cell enables us to monitor the applied *forces*, but the applied *pressure* exerted on the fibers remains unknown.

Spectral Processing. The spectral range of 1800−1200 cm^{-1} was selected, and all imaging ATR-FTIR and microscopic spectra (but not regular ATR-FTIR spectra) were baseline-corrected using the rubber-band method (5 iterations, 200 baseline points). Because varying the applied pressure also varied the intensities of the spectra, normalization was required and applied to all spectra. This was done using vector normalization. Min−max normalization was less useful because the amide I absorption is the most intense band in all spectra, and it changes in both intensity and position with pressing; normalization to this band complicates the interpretation of all other bands (including, for example, that at 1250 cm^{-1} which is not changed by pressing). After vector normalization, an offset correction was used to bring all spectra to the same zero baseline.

Principal component analysis (PCA) is used to reduce the dimensions of data into a series of orthogonal eigenvectors that are linear functions of the original variables, and which represent the directions of the greatest variances in the data, while retaining the information about the variations in data points.[36] This new space is spanned by the principal components (PCs), and most of the variations in the original data are represented by variations in the first few (one, two, or three) PCs.[37] MATLAB R2019a was used for the multivariate analysis. PCA was employed to compress the large number of correlated wavenumbers into new reduced data sets. This procedure was applied independently for different spectral regions to study the spectral changes induced by the application of pressure to the fibers. Only the first principal component (PC1) was used for the data analysis included below.

For fitting component bands to the absorbance spectrum, the band fitting feature in the OPUS 7.2 software (Bruker Optics) was used. Estimated positions of the bands were obtained from second derivatives of each spectrum. All fittings were done by the Levenberg−Marquardt method using Gaussian fitting functions, until the RMS deviation between the experimental and the fitted spectra was <0.002. No parameters (peak positions, widths, or intensities) were held fixed during the fitting procedure.

The width of the band near 1650 cm^{-1} was estimated from the second-derivative spectrum of NT2RepCT in Figure S5 and from a published spectrum (Figure 2a in ref 30) which is attributed to the silk I form.[38] In both cases, the width of the second derivative minimum was evaluated at half of its value, either using the full width for silk I or using the half-width on the high wavenumber side for NT2RepCT because this region was less affected by overlap from other bands. The half-width was converted to full width, and the full widths were multiplied by a factor of 2 to correspond to full widths in the absorption spectrum. The factor was determined from artificial curves with a Gaussian line profile and 30 cm^{-1} full width at half-height.

RESULTS AND DISCUSSION

ATR under Variable Applied Force. To study the secondary structure of protein fibers under different applied forces, ATR spectra of biomimetic artificial spider silk fibers (spun from the protein NT2RepCT[33,34]) were recorded under an increasing pressing force of the ATR accessory. Figure 1

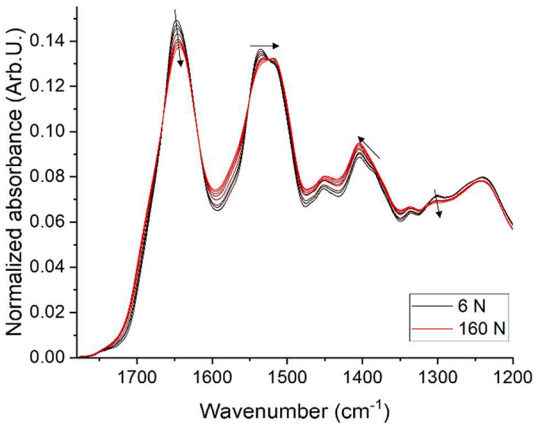

Figure 1. Normalized ATR spectra of the NT2RepCT fibers under different applied forces. The arrows indicate changes under increasing applied pressing force, from 6 N (black) to 160 N (red; the applied forces used for the intermediate curves are listed in Table S1).

shows how the normalized ATR spectra between 1750 and 1200 cm^{-1} change as the force gradually increases from 6 to 160 N on the same set of fibers, and arrows indicate the spectral changes under increasing applied force. Increasing the force applied to the fibers shifts the absorbance bands from 1652 to 1644 cm^{-1} and from 1537 to 1518 cm^{-1} and decreases the intensity of the band around 1301 cm^{-1}. The sample was released after pressing under the maximum load, and its spectrum was recorded under 6 N force, immediately after release, and again after 1 h. The results show that the spectra under released force are very similar to those acquired under the highest load, indicating an irreversible change in the secondary structure (spectra obtained after release are shown in Figure S3).

The observed spectral changes comprise three spectral regions of protein backbone absorption, which are sensitive to secondary structure:[39] amide I (centered at 1750−1600 cm^{-1} mostly representing carbonyl (C═O) stretching), amide II (centered at 1590−1470 cm^{-1} with main contributions from C−N stretching and N−H bending), and amide III (centered at 1350−1250 cm^{-1} and including more complex vibrational modes). They are assigned to secondary structures based on previous literature.[40−47] The band positions at 1652, 1537, and 1301 cm^{-1} are characteristic of α-helices. We note, however, that the silk I form of *Bombyx mori* has an infrared spectrum that is similar to that of an α-helix, although NMR evidence indicates that the structure consists of repeated type II β-turns.[38] This is conceivable because the infrared spectrum of α-helices is difficult to distinguish from that of secondary structures that are neither α-helices nor β-sheets.[41,42,44,48] Therefore, assignment of the 1652 and 1537 cm^{-1} bands to type II β-turns is also possible. Nevertheless, the small bandwidth of the 1652 cm^{-1} band in the absorption spectrum of NT2RepCT argues in favor of an assignment to α-helices. It was estimated to ∼26 cm^{-1} (see Materials and Methods

https://doi.org/10.1021/acsapm.3c01892
ACS Appl. Polym. Mater. 2023, 5, 9433−9444

section), which is somewhat less than the value of 32 cm^{-1} found for three α-helical polypeptides[49] and thus indicates a well-defined conformation. In contrast, the bandwidth of silk I was estimated to ~38 cm^{-1}, implying a more heterogeneous structure for silk I than that for NT2RepCT. A further argument for an assignment of the 1652 cm^{-1} band to α-helices is the associated absorbance decrease in the amide III spectral range at 1301 cm^{-1}, the spectral position of which is characteristic of α-helices, but not of turns.[45,47] The silk I spectrum shows instead a band at 1233 cm^{-1} [30] which is located at the low wavenumber side of the spectral range of turns.[47] Thus, we consider an assignment of the 1652 cm^{-1} band to α-helices to be the most likely but admit that it is not unequivocal, and we do not exclude the contribution of broader spectral features from other secondary structures in this spectral range because they show up less obviously in second-derivative spectra. However, to keep the text simple, we refer to this band as α-helix in the following.

With increasing force, the amide I band shifts to 1644 cm^{-1}, which is due to a decrease of the band at 1652 cm^{-1} and an increase of a component band at 1638 cm^{-1}, evident in the second derivative spectra shown in Figure S7. The 1638 cm^{-1} band and the amide II band at 1518 cm^{-1} can be assigned to β-sheets. Thus, the observed force-induced change is consistent with a transition of α-helix structures into β-sheets but could also be caused by a shape change where the dipole moments of the β-sheets are better aligned to the electric field vector than those of the α-helices under high loads due to redistribution or reshaping of the probed volume as a result of pressing as discussed in the following.

To determine whether the spectral changes are caused by changes in the protein secondary structure or emerge because of shape changes largely without secondary structure changes, caused by realignment of the transition dipoles indicative of α-helices and β-sheets under deformation of the fibers, spectra were investigated under polarized infrared illumination. Shape changes under varying applied loads are expected and reported in the literature, for example, in an ATR-FTIR study on the classification of textile fibers, including silk.[9] Under a mere shape change, the changes in s- and p-polarized spectra would mirror each other in that a change in one spectrum would correspond to a similar, but reverse, change in the other spectrum because the projections of the molecular transition dipoles on the two polarization directions are coupled. Figure 2 shows spectra of NT2RepCT fibers under different applied forces (ca. 3−88 N), obtained with nonpolarized, s-polarized, and p-polarized light. The three sets of spectra in Figure 2 were obtained from the same fibers (but each series was acquired at a new position on the fiber bundle). The changes in the polarized spectra do not mirror each other, but both spectra rather show changes that are not balanced by reverse changes in the spectrum of the other polarization. Corresponding spectra for natural fibers are shown in Figure S4, and we note that similar changes can be observed in the latter, though these are smaller, and thus the natural fiber appears to be more resistant to pressing (a figure comparing the spectra is included as Figure S5). These results confirm a genuine structural transition under an increasing applied force. The bands near 1750 cm^{-1} (and which are absent from the data in Figure 1) are probably caused by lipopolysaccharides in the fiber, which are common contaminants from the *E. coli* production system.[50,51] In Figure 2, the changes in the nonpolarized spectra appear to be smaller than for the polarized measurements, whereas under ideal conditions, the nonpolarized spectrum should be the average of the two polarized spectra. In the interpretation of these spectra, it is important to remember that several issues will affect the resulting spectra and a comparison between them. (i) The sets of spectra for the different polarizations were obtained in separate experiments for technical reasons (as explained above). This is the reason the spectra between the sets were acquired at slightly different applied forces (see Table S1). This cannot fully explain the differences, but might contribute to them. (ii) As the applied force increases, the absolute intensities of the spectra increase due to the larger contact area of the fibers on the prism, but each spectrum is normalized individually, so direct quantitative comparisons from the shown spectra are difficult. (iii) The penetration of the p-polarized beam into the sample is larger than for the s-polarized beam, so the absolute changes can be different for the two polarizations due to the changes in geometry upon deformation. This implies that for normalized spectra, the nonpolarized measurement is a weighted average of the two polarizations, where they do not contribute equally. A comparison of nonpolarized spectra with averages of s- and p-polarized spectra is included in Figure S6. (iv) Finally, the wire grid polarizers used for polarization are not ideal polarizers, and beam focusing in the MIRacle ATR accessory does not fully maintain polarization, so some mixing should be expected. All of these factors make quantitative comparisons of the intensity variations between the spectra in Figure 2 (and Figure S4) difficult. Irrespective of the aforementioned issues, the conclusion that the peak *shifts* confirms a genuine structural transition under an increasing applied force remains unaffected.

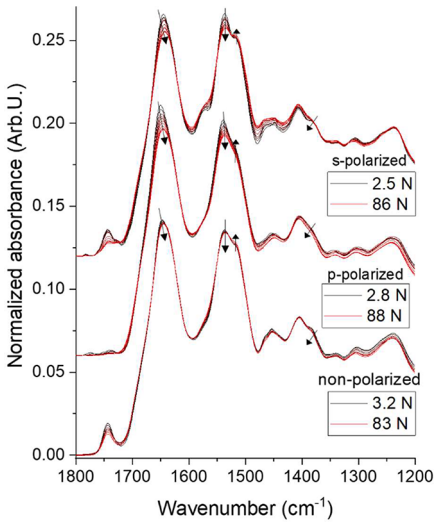

Figure 2. Normalized ATR spectra of NT2RepCT fibers under different applied forces probed with light using different polarizations. Arrows indicate changes upon increasing applied pressing force, from ca. 3 to ca. 88 N (the applied forces for the intermediate curves are listed in Table S1). The two sets of polarized spectra are vertically offset by 0.06 and 0.12 units, respectively, for clarity.

For a more thorough assessment of the spectral changes, we need to identify the relative contributions from different structural motifs to each spectrum.

Spectral band fitting can be used to identify and quantify secondary structure elements of proteins, and for a more precise analysis, the three amide regions of the spectra were fitted to identify contributions from different secondary

https://doi.org/10.1021/acsapm.3c01892
ACS Appl. Polym. Mater. 2023, 5, 9433−9444

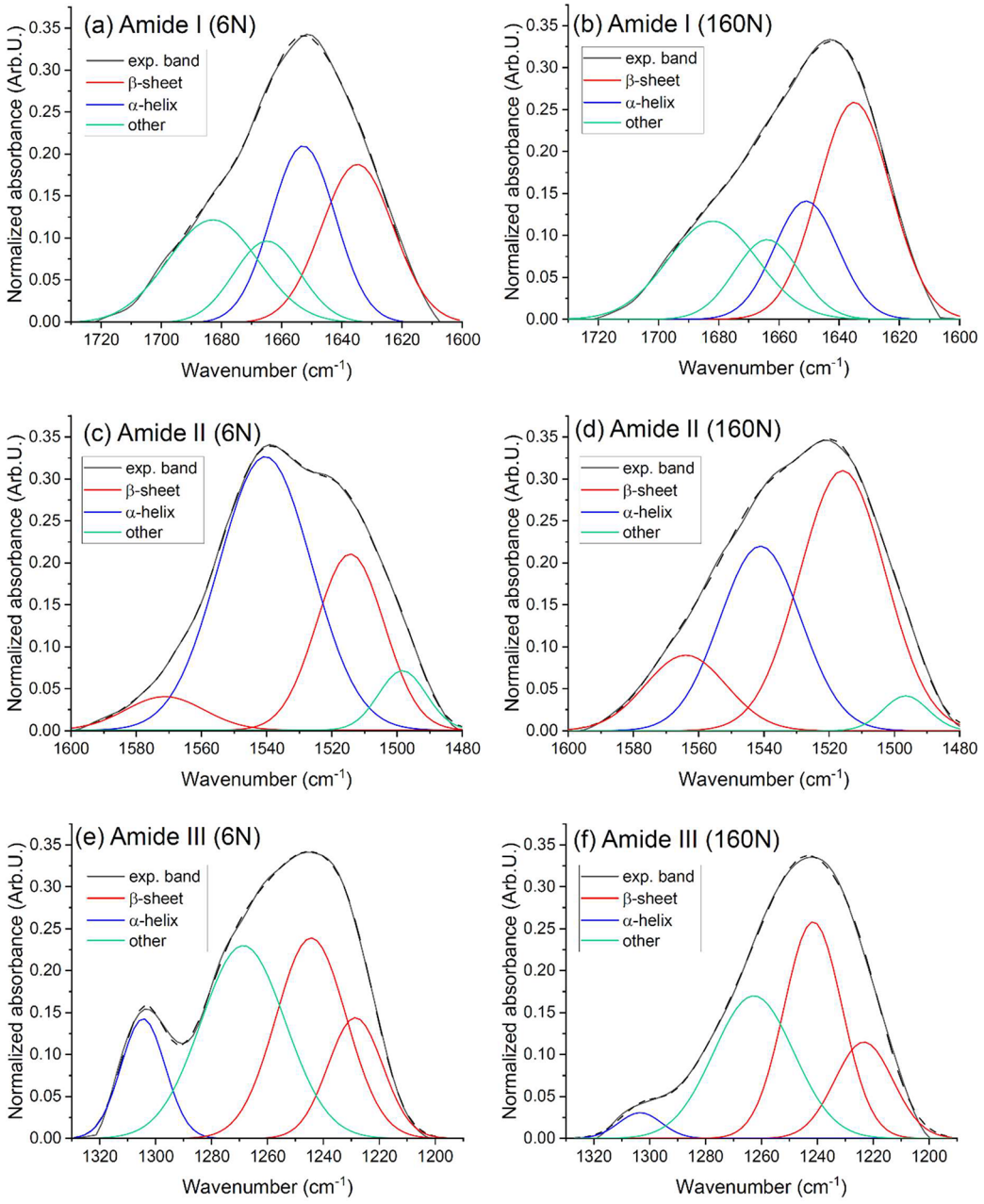

Figure 3. (a–f) Band shape analysis by fitting the component bands of the ATR spectra of a NT2RepCT fiber sample under low (6 N) and high (160 N) pressing forces for the amide I–III regions.

structure motifs. We used second derivatives (Figure S7) to find the band positions to feed into the fitting process. Figure 3 shows the results of this analysis for ATR spectra of artificial fibers (NT2RepCT), in this case under 6 and 160 N applied forces, for the three amide regions. Secondary structure transformations are confirmed by comparing the intensities of bands associated with α-helix and β-sheet structure, under different applied forces. The integrated areas of the amide component bands were determined to quantitatively assess the structural transformation rate in the silk fiber proteins. For each amide band, the main contributions to each secondary structure type were used to calculate a β/α ratio. These bands are centered at 1652 ± 2 cm^{-1} (α) and 1634 ± 3 cm^{-1} (β) in the amide I region, at 1538 ± 4 cm^{-1} (α) and 1511 ± 3 cm^{-1} (β) in the amide II region, and at 1301 ± 3 cm^{-1} (α) and 1241 ± 2 cm^{-1} (β) in the amide III region. Figure 4 shows the ratios of the integrated band intensities in each region (giving β/α structural ratios) for different applied forces. These results are consistent for the three amide bands and clearly show how the structure transformation from α-helix to β-sheet proceeds under the increasing applied force.

Reversibility of the Structural Changes. To assess whether elastic or plastic deformation occurs under applied load, NT2RepCT fibers were measured at a low (2–3 N) and high applied force (80–85 N) and thereafter released to a low pressing force (3–4 N), and spectra were collected continuously every 5 min for 1 h. Figure 5 shows spectra under low and high pressing force, and after 5 and 60 min, respectively, after releasing the high pressing force. The data show not only that the secondary structure changes are partially reversible but also that there is very little difference between the spectra obtained 5 and 60 min after relaxing the

https://doi.org/10.1021/acsapm.3c01892
ACS Appl. Polym. Mater. 2023, 5, 9433–9444

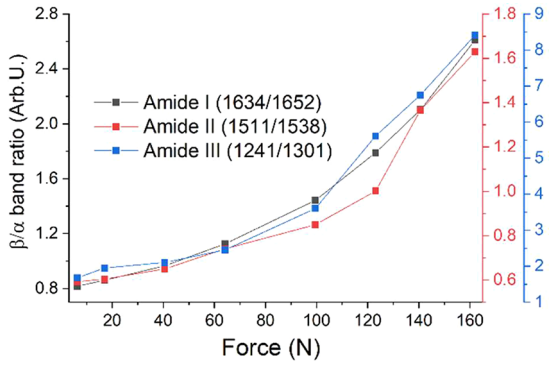

Figure 4. Summary of the band ratios (β/α structural ratios) of integrated bands obtained by curve fitting in each amide region (see Figure 3) as an indicator of the α-helix to β-sheet transformation. Note the different vertical scales for each amide band.

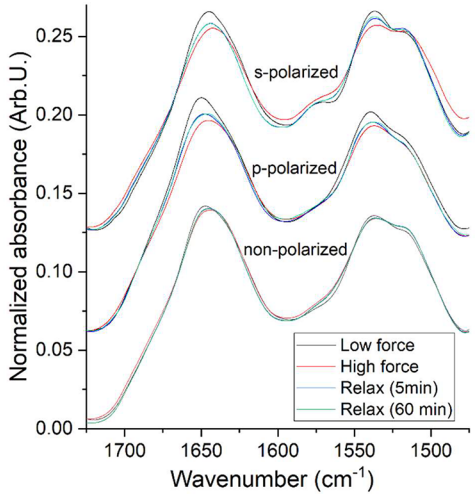

Figure 5. Normalized ATR spectra of the NT2RepCT fibers under low and high pressing force and in a relaxed state 5 and 60 min after releasing the high pressing force.

pressure and that the plastic changes in the fibers occur immediately, with little creep. This is consistent with the normal relaxation times in spider silk[52] and also in agreement with previous studies, finding that macroscopic strain was immediately reflected in microscopic structural changes.[53]

To better understand the reversibility, averages of 20 spectra of relaxed fibers (after release of the high pressing force; see Figure 5) were calculated for each polarization. These average spectra were then compared to similarly averaged spectra of the NT2RepCT fibers under pressure, and principal component analysis (PCA) was applied to analyze the data for each polarization separately (see Figure 6). The first principal component (PC1) represents the absorbance differences between the averaged spectra (under zero and high applied force, respectively) and was used as an indicator for the reversibility. The PCA data were normalized so that the value at the lowest force was selected as the minimum (zero) and that at the highest force as maximum (set to 1). Figure 6 shows the normalized PC1 values for different pressing forces and for data obtained under both unpolarized and polarized illumination.

The results show that spectra are more reversible in the s-polarized (55.7%) direction in comparison with either the nonpolarized (13.2%) or p-polarized (23.9%) spectra. There

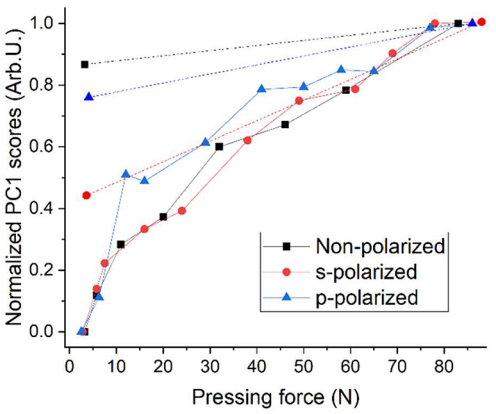

Figure 6. Normalized PC1 for whole spectra for different applied forces and different polarizations, indicating the degree of spectral change measured from low to high pressing force. The applied pressure was released after the highest force, and the samples were allowed to relax to a low force (in the range 3−5 N), indicated by the data points on the left, connected by dashed lines.

are two possible explanations for these differences in the reversibility with the polarization direction. First, the samples stick to the prism surface under a high pressing force, which can constrain the expansion parallel to the prism surface, in comparison with the change perpendicular to the prism surface. Second, the difference can also be a result of the different penetration depths of the two polarization directions, where nonpolarized and p-polarized light penetrate deeper than s-polarized light. Thus, nonpolarized and p-polarized light probe a greater volume (more material) in comparison to s-polarized light. The effects of pressing and releasing are different for the two polarizations depending on the changing shape of the fiber under applied pressure, but a precise analysis of these effects would require detailed knowledge about the geometrical changes with increasing pressure.

Further, not all bands show the same degree of reversibility for each polarization. To distinguish the degree of reversibility of each band, we used second derivatives to identify 18 different spectral band positions, including all three amide band regions. Then, each spectrum was fitted using these component bands, and PCA was applied to each component band, for the nonpolarized spectra and the two sets of polarized spectra, separately. After that, PC1 was normalized for each component band (similarly to the analysis for whole spectra above summarized in Figure 6, but here the analysis is for each band separately), and a measure of the degree of reversibility for each band was determined from the changes in the PC1 magnitudes. These results are listed in Table S3 and displayed in Figure 7, where four bands show distinct irreversibility. The intensities of the bands centered at 1635 (amide I) and 1381 cm^{-1} (CH_2 and/or CH_3 bending) of the β-sheet structure were irreversibly increased, and the intensities of the bands at 1531 cm^{-1} (amide II) and 1307 cm^{-1} (amide III) of the α-helix structure were irreversibly decreased. Thus, these results also support the view that permanent changes resulting in a transformation from α-helix to β-sheet structure follow after applied pressure and deformation of the samples.

Polyalanine Bands. Previous studies have found that a backbone vibrational mode in β-sheet polyalanine nanocrystals appears at 965 cm^{-1} if no external load is applied and that it shifts under applied stress. This band can thus be used as an

https://doi.org/10.1021/acsapm.3c01892
ACS Appl. Polym. Mater. 2023, 5, 9433−9444

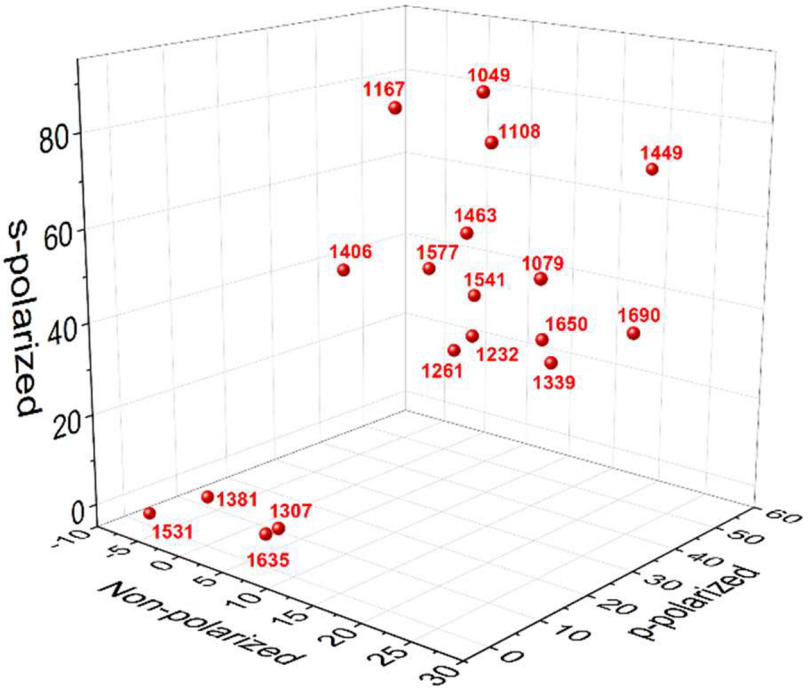

Figure 7. Reversibility percentages of the fitted component bands. The percentages are plotted along the three Cartesian axes for the different polarizations used. The group of four bands in the lower left corner (1307, 1381, 1531, and 1635 cm^{-1}; see text for details) differ from the other bands in that they have much lower reversibility.

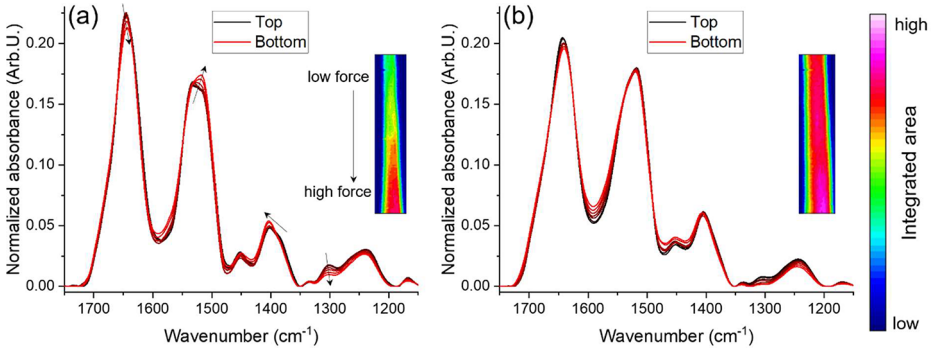

Figure 8. Averaged spectra of eight different segments of a single fiber sample obtained by ATR micro-IR imaging under (a) a force gradient under low average applied force, on average 10 N, where arrows indicate the changes occurring in the spectra upon moving in the direction of increasing pressing force, i.e., from top to bottom in the inset image, and (b) spectra of the fiber at high average pressing force, ca. 450 N. Each image was divided into eight equal-length parts along the fiber direction, and average spectra of each part were obtained. Colors in the inset images represent total IR intensity (in arbitrary units) indicating strong (red), weak (green), or no (blue) contact between fiber and IRE.

internal molecular sensor of externally applied pressure.[19,53] However, macroscopic stress applied to the fiber does not necessarily translate to a proportional crystal stress,[19] and the existence of prestress in silk, with ensuing decrease in nanocrystal stress upon increasing external stress,[54] complicates the use of this band as an indicator of external stress. Using second derivatives, the position of this band is also resolved in our data. For measurements on 5−8 NT2RepCT fibers, the position of this polyalanine band moves from 961 to 967 cm^{-1} as the applied force is increased from 6 to 64 N, but upon further increase, the band reverts to 965 cm^{-1}, to remain there, also as the clamp is released to 7 N after reaching the maximum pressure (see Figure S8 and Table S4). The initial increase is in qualitative agreement with the changes observed by Anton et al.,[19] upon applying increasing hydrostatic stress to silk fibers. However, whereas the isotropically acting hydrostatic pressure resulted in completely reversible shifts of this band, the plastic deformation induced by the press in our ATR-FTIR setup acts differently and, like other spectral changes induced by the pressing force, does not result in fully reversible changes. Nevertheless, the observed band shift supports the interpretation of our data in terms of structural changes induced by the externally applied force and the irreversibility of these changes at high applied forces.

ATR Imaging. Further, micro-IR imaging in the ATR mode was used to confirm the ATR results mentioned above. Figure 8 shows ATR spectra of a single NT2RepCT fiber under different pressing forces (the images in Figure 8 are selected from IR images, which are provided in full in Figure S9). In Figure 8a the average applied force is 10 N, while in Figure 8b it is ca. 450 N. Because of small imperfections in the measurement (misalignment, dust, fiber thickness variations, etc.) in combination with a pivoting head at the press end, the resulting force is not homogeneous over the sample but results

https://doi.org/10.1021/acsapm.3c01892
ACS Appl. Polym. Mater. 2023, 5, 9433−9444

in a force gradient across the image, with the force increasing from top to the bottom in the inset images in Figure 8. To analyze the results, each IR image of the fiber was divided into eight equal-length segments along the fiber length. The arrows in the spectra in Figure 8a indicate changes as they occur when moving from the top to the bottom part of the adjacent fiber image, and the average spectrum of each part is shown in the figure. Figure 8a shows a secondary structure transformation of the silk under an increasing pressing force along the fiber. The spectral changes that are indicated by the arrows are qualitatively very similar to the changes from α-helix to β-sheet observed with the regular (nonimaging) ATR method in the previous analysis. Under high pressing force (Figure 8b), the structure of the silk fiber in the entire imaging area is transformed into largely the same, presumably β-sheet structure, with much less variation between the spectra from different segments of the fiber.

Principal component analysis (PCA) was applied to visualize the results obtained so far. In this evaluation, all spectra were first divided into three groups, where spectra from Figures 1 and S3 form one group and spectra from Figures 8a and 8b form separate groups. Thereafter, the spectra were split into three spectral ranges: amide I (1770−1600 cm^{-1}), amide II (1590−1470 cm^{-1}), and amide III (1350−1250 cm^{-1}); PCA was applied to each amide band separately, for all spectra. This was thus repeated for the eight different applied pressures shown in Figure 1, for the spectrum at low force after release (shown in Figure S3) and for each of the spectra from the eight segments in Figures 8a and 8b), and the resulting data were used to assemble Figure 9. For each spectral range region, PC1 accounts for 96−98% of the variance in the IR data. In Figure 9, each spectrum is thus represented as a point, the location of which is defined by the loadings of the first principal components in each of the three spectral regions (amide I−III). This analysis demonstrates that the same structural transformation is occurring under increasing pressing force both in the conventional ATR measurements (red) and under the force gradients in imaging ATR (purple). The result from the released sample in the ATR measurement (blue) confirms that the fibers' secondary structure does not change after releasing the pressure on the sample and that it remained in β-sheet structure. Results from the highly pressed sample in the imaging ATR mode (green) confirmed that there is a final secondary structure (β-sheet) that the sample will reach under high pressure.

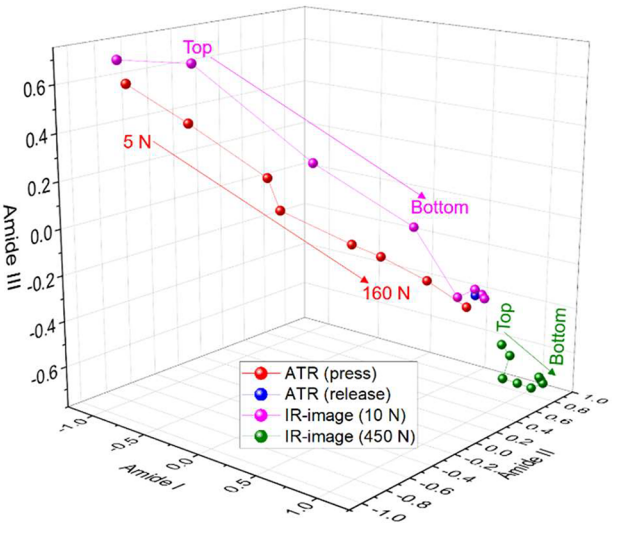

Figure 9. Mapping of PC1 of the three amide regions for each measurement. Red and blue markers correspond to the data in Figures 1 and S3, respectively; purple markers are data from Figure 8a, and the green markers correspond to the data in Figure 8b (some markers are partially overlapping). The red arrow indicates the direction of increasing the pressing force in the data from Figure 1. The purple and green arrows indicate directions of increasing pressing force (from top to bottom) in the insets in Figures 8a and 8b, respectively.

IR Microspectroscopy. For comparison, IR microspectroscopy in reflection mode was also applied to study the secondary structure of the spider silk fibers. This technique has been used in previous studies to verify deviations to spectra obtained with the ATR-FTIR technique,[31,32] and we proceed to do the same to verify our results obtained by ATR-FTIR and to assess the consistency with existing literature. Figure 10a shows the normalized averaged spectra from two regions

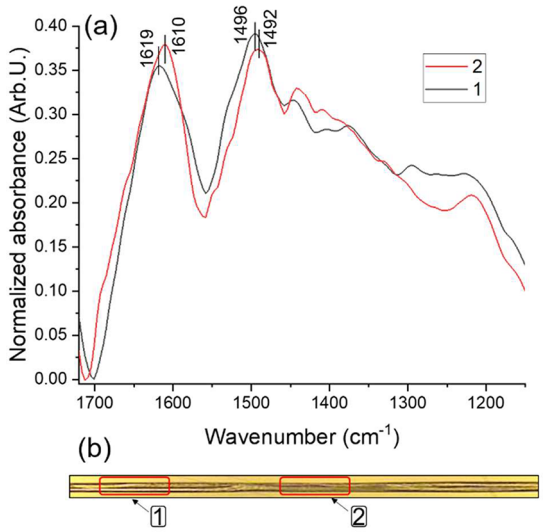

Figure 10. (a) Normalized and averaged spectra of the two indicated areas of the NT2RepCT fiber shown in (b), obtained by IR microspectroscopy in reflectance mode with a gold-coated slide as the substrate. The central part of the fiber (region 2) was pressed to ca. 80 N in an ATR accessory before the IR microspectroscopy analysis while region 1 remained untreated.

of an NT2RepCT fiber, which was mounted in the ATR accessory under a force of ca. 80 N and then transferred to a gold-coated glass slide for IR imaging. The central portion of the fiber in Figure 10b was pressed, and a comparison of the spectra from the pressed (2) and nonpressed (1) regions reveals clear differences. The maxima of the amide I (1619 → 1610 cm^{-1}) and amide II (1496 → 1492 cm^{-1}) bands are shifted from the unaffected to the pressed area. These spectral changes are qualitatively similar to the shifts presented in the ATR section above, induced by increasing pressing force, which confirmed that the α-helix structure turns into β-sheet in the twisted region. This test shows that the distribution of the total intensity is different in the pressed region compared to the unaffected parts of the fiber and that the intensity of the bands associated with the β-sheet structure is higher in the pressed area.

We extended this comparison to consider a twisted natural spider silk fiber, and Figure 11a shows normalized averaged

https://doi.org/10.1021/acsapm.3c01892
ACS Appl. Polym. Mater. 2023, 5, 9433−9444

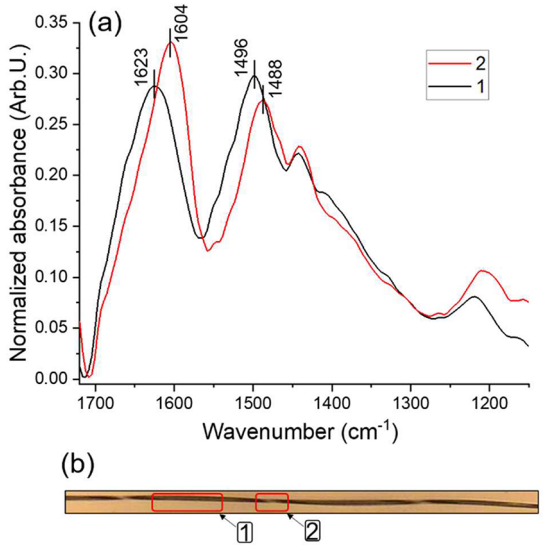

Figure 11. (a) Normalized and averaged spectra of the indicated areas of a spider major ampullate silk fiber shown in (b), obtained by infrared microspectroscopy in reflectance mode, with a gold-coated slide as the substrate. Regions 1 and 2 in (b) represent nontwisted and twisted regions of the fiber, respectively.

spectra from two selected areas of a spider major ampullate silk fiber, as indicated in the optical image in Figure 11b. Area (1) is the normal (nontwisted) fiber structure, and area (2) is a twisted part of the fiber. A comparison of the averaged spectra from these two regions shows shifts that are similar to those observed in previous experiments. The maxima of the amide I (1619 → 1608 cm^{-1}) and amide II (1496 → 1482 cm^{-1}) bands are shifted from the normal to the twisted area. Just as in the example shown in Figure 10, the distributions of the total intensities are different in the twisted and the normal regions, with bands associated with β-sheet structure higher in the twisted parts of the fiber compared to the natural, nontwisted, parts.

Sampling Method Effects. Comparing the spectra obtained from conventional ATR, ATR imaging, and the reflectance microspectroscopy results, the amide band peaks are consistently shifted to lower wavenumbers under applied external stress, and this shift is qualitatively similar in all cases. From component fitting of the amide bands, and also based on other spectral features, these changes are associated with transformations from α-helix to β-sheet secondary structure, and it is also clear that pressing the sample to the IRE in the ATR accessory contributes to this transition. While the data obtained from the different sampling methods do not represent the same samples, the differences in the spectra from the respective sampling methods still deserve some comment. Most notable are the lower wavenumbers of the amide I band peak positions in the IR microspectroscopy results in Figures 10 and 11, as compared to the band positions observed in the ATR measurements shown in the previous section. There are two possible explanations for this difference, either the geometry of the samples or optical effects specific to the two sampling methods, as discussed in the following.

(i) Refraction and scattering of beams in fibers, in combination with variations in refractive index with wavelength and cross section, will affect the spectral data.[55] It has been demonstrated that a cylindrical shape distorts the optical fields in and around fibers, resulting in significant spectral distortion, particularly if the fiber thickness approaches the used wavelength.[56] This is indeed the situation here, with fibers of ca. 10 and 16 μm diameter, which is of the order of the wavelengths in the mid-IR region. This will affect both transmission and ATR measurements, but in different ways, depending on the differences in beam paths and probed volumes in the fibers. With irregularly shaped fibers, the effects on the resulting spectra are also very difficult to model or predict.

(ii) The optical features of ATR measurements are such that both peak intensities and peak positions can be distorted when comparing to, for example, transmission spectra.[57] The alteration of peak intensities is a result of the wavelength-dependent penetration depth of the evanescent wave into the sample. This is routinely compensated for with a linear correction over the entire spectrum (also in our spectra). Upon comparison, however, the peak positions of ATR spectra are normally also shifted to lower wavenumbers, compared to transmission (or ideal absorption) spectra. These shifts are opposite to those observed upon comparison of our ATR spectra with the reflectance microspectroscopy results shown in Figures 10 and 11, but the reflection−absorption spectra obtained by IR microspectroscopy are also not ideal absorption spectra, so predictions assuming ideal spectra in this case are not *a priori* applicable. The peak shifts observed in ATR spectra can be accounted for by considering a contribution to the penetration depth (d_p) from the rapid variation of the sample refractive index (n_2) with wavelength near absorption bands (the correction of which is often termed "extended", "advanced", or "anomalous dispersion" ATR correction). This causes the effective path length in the sample to differ from d_p,[58] though this distinction is often ignored. The shift in peak position can be understood as a modification of the absorption coefficient of the sample, $\alpha(\lambda)$, from which the peak positions are normally found by looking for local maxima. With a penetration depth depending on wavelength, and anomalous dispersion (increasing refractive index with wavelength) near absorption bands, it is not $\alpha(\lambda)$, but the product $\alpha(\lambda)d_p n_2$, which determines the peak positions. This results in a shift to lower frequencies (wavenumbers), and more so for strong absorption bands, when comparing ATR data with transmission or ideal absorption spectra. Procedures for compensation of such shifts, applicable to proteins, and specifically for the amide bands, are described in the literature, though these are nontrivial and require knowledge about the samples which is not always available.[59−61] Corrections for this effect have not been implemented in our spectra because this requires that the refractive indices of the sample and substrate are known, but the refractive index for the sample is generally the most uncertain parameter in the correction, and even more so for fibers. The refractive index of a fiber is usually not constant across the fiber diameter, even in areas where there are no twists or bends, so this will be very difficult to calculate.[56] In addition, the cross-sectional shape of a fiber means that there is a path-length difference variation across the sample, exacerbating the difficulties in calculating the ATR corrections.

https://doi.org/10.1021/acsapm.3c01892
ACS Appl. Polym. Mater. 2023, 5, 9433−9444

While these issues might complicate, or prevent, direct and detailed comparison of results between different sampling techniques, our data unambiguously demonstrate that pressure-induced changes are present in the ATR spectra and that qualitatively similar effects are seen in single fibers under local strain in IR microspectroscopy. We observed these structural changes while operating the ATR accessories according to the recommendations of the respective manufacturers. In contrast, our recent NT2RepCT spectra using a different ATR accessory (Platinum ATR, Bruker) produced typical low-force second-derivative spectra in which the β-sheet shoulder is considerably less intense than the α-helix band.[34,62,63] Discrepancies between different ATR studies could therefore arise due to the use of different ATR accessories.

CONCLUSIONS

Based on a series of different experiments, we demonstrate that the use of ATR-FTIR as a sampling method for studying the secondary structure of spider silk fibers can induce structural changes in both natural and synthetic spider silk fibers, as a result of pressing the sample against the surface of the internal reflection element in the ATR-FTIR accessory. Experiments under different applied loads, in combination with polarization analysis and fitting of spectral components, demonstrate that the induced structural changes correspond to a transformation from α-helix to β-sheet secondary structure and that these structural changes are largely irreversible. Both ATR-FTIR imaging and IR microspectroscopy confirm these observations. Thus, when using the ATR-FTIR technique with spider silk fibers, the possibility of force-induced structural changes should be taken into account, and great care should be applied in experimentation and in the interpretation of the results.

ASSOCIATED CONTENT

Supporting Information

The Supporting Information is available free of charge at https://pubs.acs.org/doi/10.1021/acsapm.3c01892.

Schematic of the load cell, additional data on applied loads, comparisons of polarized and nonpolarized spectra, comparisons of spectra from natural and synthetic spider fibers, second derivatives of amide I, II, and III spectra, reversibility percentages for identified bands, polyalanine band spectra, additional ATR-FTIR imaging data (PDF)

AUTHOR INFORMATION

Corresponding Author

Thomas Ederth − *Division of Biophysics and Bioengineering, IFM, Linköping University, 581 83 Linköping, Sweden;* orcid.org/0000-0002-1639-5735; Email: thomas.ederth@liu.se

Authors

Mohammad Javad Jafari − *Division of Biophysics and Bioengineering, IFM, Linköping University, 581 83 Linköping, Sweden;* orcid.org/0000-0003-3899-4891

Fredrik G. Bäcklund − *Department of Biosciences and Nutrition, Karolinska Institutet, 141 86 Huddinge, Sweden; RISE Research Institutes of Sweden, Division Materials and Production, Department of Polymers, Fibers and Composites, 431 53 Mölndal, Sweden*

Tina Arndt − *Department of Biosciences and Nutrition, Karolinska Institutet, 141 86 Huddinge, Sweden*

Benjamin Schmuck − *Department of Biosciences and Nutrition, Karolinska Institutet, 141 86 Huddinge, Sweden; Department of Anatomy, Physiology and Biochemistry, Swedish University of Agricultural Sciences, 750 07 Uppsala, Sweden;* orcid.org/0000-0003-4021-6458

Gabriele Greco − *Department of Anatomy, Physiology and Biochemistry, Swedish University of Agricultural Sciences, 750 07 Uppsala, Sweden;* orcid.org/0000-0003-3356-7081

Anna Rising − *Department of Biosciences and Nutrition, Karolinska Institutet, 141 86 Huddinge, Sweden; Department of Anatomy, Physiology and Biochemistry, Swedish University of Agricultural Sciences, 750 07 Uppsala, Sweden;* orcid.org/0000-0002-1872-1207

Andreas Barth − *Department of Biochemistry and Biophysics, Stockholm University, 106 91 Stockholm, Sweden;* orcid.org/0000-0001-5784-7673

Complete contact information is available at: https://pubs.acs.org/10.1021/acsapm.3c01892

Notes

The authors declare no competing financial interest.

REFERENCES

(1) Arakawa, K.; Kono, N.; Malay, A. D.; Tateishi, A.; Ifuku, N.; Masunaga, H.; Sato, R.; Tsuchiya, K.; Ohtoshi, R.; Pedrazzoli, D.; Shinohara, A.; Ito, Y.; Nakamura, H.; Tanikawa, A.; Suzuki, Y.; Ichikawa, T.; Fujita, S.; Fujiwara, M.; Tomita, M.; Blamires, S. J.; Chuah, J.-A.; Craig, H.; Foong, C. P.; Greco, G.; Guan, J.; Holland, C.; Kaplan, D. L.; Sudesh, K.; Mandal, B. B.; Norma-Rashid, Y.; Oktaviani, N. A.; Preda, R. C.; Pugno, N. M.; Rajkhowa, R.; Wang, X.; Yazawa, K.; Zheng, Z.; Numata, K. 1000 spider silkomes: Linking sequences to silk physical properties. *Science Advances* **2022**, *8* (41), No. eabo6043.

(2) Greco, G.; Mirbaha, H.; Schmuck, B.; Rising, A.; Pugno, N. M. Artificial and natural silk materials have high mechanical property variability regardless of sample size. *Sci. Rep.* **2022**, *12* (1), 3507.

(3) Gu, Y.; Yu, L.; Mou, J.; Wu, D.; Zhou, P.; Xu, M. Mechanical properties and application analysis of spider silk bionic material. *e-Polym.* **2020**, *20* (1), 443−457.

(4) Koh, L.-D.; Cheng, Y.; Teng, C.-P.; Khin, Y.-W.; Loh, X.-J.; Tee, S.-Y.; Low, M.; Ye, E.; Yu, H.-D.; Zhang, Y.-W.; Han, M.-Y. Structures, mechanical properties and applications of silk fibroin materials. *Prog. Polym. Sci.* **2015**, *46*, 86−110.

(5) Barth, A. Infrared spectroscopy of proteins. *Biochimica et Biophysica Acta (BBA) - Bioenergetics* **2007**, *1767* (9), 1073−1101.

(6) Byler, D. M.; Susi, H. Examination of the secondary structure of proteins by deconvolved FTIR spectra. *Biopolymers* **1986**, *25* (3), 469−487.

(7) Wilcox, K. E.; Blanch, E. W.; Doig, A. J. Determination of Protein Secondary Structure from Infrared Spectra Using Partial Least-Squares Regression. *Biochemistry* **2016**, *55* (27), 3794−3802.

(8) Fang, G.; Huang, Y.; Tang, Y.; Qi, Z.; Yao, J.; Shao, Z.; Chen, X. Insights into Silk Formation Process: Correlation of Mechanical Properties and Structural Evolution during Artificial Spinning of Silk Fibers. *ACS Biomater. Sci. Eng.* **2016**, *2* (11), 1992−2000.

(9) Peets, P.; Leito, I.; Pelt, J.; Vahur, S. Identification and classification of textile fibres using ATR-FT-IR spectroscopy with chemometric methods. *Spectrochimica Acta Part A: Molecular and Biomolecular Spectroscopy* **2017**, *173*, 175−181.

(10) Wang, Q.; McArdle, P.; Wang, S. L.; Wilmington, R. L.; Xing, Z.; Greenwood, A.; Cotten, M. L.; Qazilbash, M. M.; Schniepp, H. C. Protein secondary structure in spider silk nanofibrils. *Nat. Commun.* **2022**, *13* (1), 4329.

(11) Boulet-Audet, M.; Lefèvre, T.; Buffeteau, T.; Pézolet, M. Attenuated Total Reflection Infrared Spectroscopy: An Efficient Technique to Quantitatively Determine the Orientation and Conformation of Proteins in Single Silk Fibers. *Appl. Spectrosc.* **2008**, *62* (9), 956−962.
(12) Carissimi, G.; Baronio, C. M.; Montalbán, M. G.; Víllora, G.; Barth, A. On the Secondary Structure of Silk Fibroin Nanoparticles Obtained Using Ionic Liquids: An Infrared Spectroscopy Study. *Polymers* **2020**, *12* (6), 1294.
(13) Marsh, D. Quantitation of Secondary Structure in ATR Infrared Spectroscopy. *Biophys. J.* **1999**, *77* (5), 2630−2637.
(14) Belbachir, K.; Lecomte, S.; Ta, H.-P.; Petibois, C.; Desbat, B. Orientation of molecular groups of fibers in nonoriented samples determined by polarized ATR-FTIR spectroscopy. *Anal. Bioanal. Chem.* **2011**, *401* (10), 3263−3268.
(15) Boulet-Audet, M.; Vollrath, F.; Holland, C. Identification and classification of silks using infrared spectroscopy. *Journal of Experimental Biology* **2015**, *218* (19), 3138−3149.
(16) Lyman, D. J.; Schofield, P. Attenuated Total Reflection Fourier Transform Infrared Spectroscopy Analysis of Human Hair Fiber Structure. *Appl. Spectrosc.* **2008**, *62* (5), 525−535.
(17) Percot, A.; Colomban, P.; Paris, C.; Dinh, H. M.; Wojcieszak, M.; Mauchamp, B. Water dependent structural changes of silk from Bombyx mori gland to fibre as evidenced by Raman and IR spectroscopies. *Vib. Spectrosc.* **2014**, *73*, 79−89.
(18) Taddei, P.; Monti, P.; Freddi, G.; Arai, T.; Tsukada, M. IR study on the binding mode of metal cations to chemically modified Bombyx mori and Tussah silk fibres. *J. Mol. Struct.* **2003**, *651*−*653*, 433−441.
(19) Anton, A. M.; Kossack, W.; Gutsche, C.; Figuli, R.; Papadopoulos, P.; Ebad-Allah, J.; Kuntscher, C.; Kremer, F. Pressure-Dependent FTIR-Spectroscopy on the Counterbalance between External and Internal Constraints in Spider Silk of Nephila pilipes. *Macromolecules* **2013**, *46* (12), 4919−4923.
(20) Ene, R.; Krywka, C.; Kang, S.-G.; Papadopoulos, P.; Burghammer, M.; Di Cola, E.; Müller, M.; Kremer, F. Structure changes in Nephila dragline: The influence of pressure. *Polymer* **2012**, *53* (24), 5507−5512.
(21) Yazawa, K.; Hidaka, K. Pressure- and humidity-induced structural transition of silk fibroin. *Polymer* **2020**, *211*, 123082.
(22) He, Z.; Liu, Z.; Zhou, X.; Huang, H. Low pressure-induced secondary structure transitions of regenerated silk fibroin in its wet film studied by time-resolved infrared spectroscopy. *Proteins: Struct., Funct., Bioinf.* **2018**, *86* (6), 621−628.
(23) van de Weert, M.; Haris, P. I.; Hennink, W. E.; Crommelin, D. J. A. Fourier Transform Infrared Spectrometric Analysis of Protein Conformation: Effect of Sampling Method and Stress Factors. *Anal. Biochem.* **2001**, *297* (2), 160−169.
(24) Van Nimmen, E.; De Clerck, K.; Verschuren, J.; Gellynck, K.; Gheysens, T.; Mertens, J.; Van Langenhove, L. FT-IR spectroscopy of spider and silkworm silks: Part I. Different sampling techniques. *Vib. Spectrosc.* **2008**, *46* (1), 63−68.
(25) Careri, G.; Gratton, E.; Yang, P. H.; Rupley, J. A. Correlation of IR spectroscopic, heat capacity, diamagnetic susceptibility and enzymatic measurements on lysozyme powder. *Nature* **1980**, *284* (5756), 572−573.
(26) Goormaghtigh, E.; Raussens, V.; Ruysschaert, J.-M. Attenuated total reflection infrared spectroscopy of proteins and lipids in biological membranes. *Biochimica et Biophysica Acta (BBA) - Reviews on Biomembranes* **1999**, *1422* (2), 105−185.
(27) Baker, M. J.; Trevisan, J.; Bassan, P.; Bhargava, R.; Butler, H. J.; Dorling, K. M.; Fielden, P. R.; Fogarty, S. W.; Fullwood, N. J.; Heys, K. A.; Hughes, C.; Lasch, P.; Martin-Hirsch, P. L.; Obinaju, B.; Sockalingum, G. D.; Sulé-Suso, J.; Strong, R. J.; Walsh, M. J.; Wood, B. R.; Gardner, P.; Martin, F. L. Using Fourier transform IR spectroscopy to analyze biological materials. *Nat. Protoc.* **2014**, *9* (8), 1771−1791.
(28) Smith, B. C. *Fundamentals of Fourier Transform Infrared Spectroscopy*; CRC Press: Boca Raton, FL, 2011.
(29) Colomban, P.; Gouadec, G. Raman and IR micro-analysis of high performance polymer fibres tested in traction and compression. *Compos. Sci. Technol.* **2009**, *69* (1), 10−16.
(30) Ling, S.; Qi, Z.; Knight, D. P.; Shao, Z.; Chen, X. Synchrotron FTIR Microspectroscopy of Single Natural Silk Fibers. *Biomacromolecules* **2011**, *12* (9), 3344−3349.
(31) Peets, P.; Kaupmees, K.; Vahur, S.; Leito, I. Reflectance FT-IR spectroscopy as a viable option for textile fiber identification. *Heritage Science* **2019**, *7* (1), 93.
(32) Badillo-Sanchez, D.; Chelazzi, D.; Giorgi, R.; Cincinelli, A.; Baglioni, P. Understanding the structural degradation of South American historical silk: A Focal Plane Array (FPA) FTIR and multivariate analysis. *Sci. Rep.* **2019**, *9* (1), 17239.
(33) Andersson, M.; Jia, Q.; Abella, A.; Lee, X.-Y.; Landreh, M.; Purhonen, P.; Hebert, H.; Tenje, M.; Robinson, C. V.; Meng, Q.; Plaza, G. R.; Johansson, J.; Rising, A. Biomimetic spinning of artificial spider silk from a chimeric minispidroin. *Nat. Chem. Biol.* **2017**, *13* (3), 262−264.
(34) Schmuck, B.; Greco, G.; Barth, A.; Pugno, N. M.; Johansson, J.; Rising, A. High-yield production of a super-soluble miniature spidroin for biomimetic high-performance materials. *Mater. Today* **2021**, *50*, 16−23.
(35) Schmuck, B.; Greco, G.; Bäcklund, F. G.; Pugno, N. M.; Johansson, J.; Rising, A. Impact of physio-chemical spinning conditions on the mechanical properties of biomimetic spider silk fibers. *Communications Materials* **2022**, *3* (1), 83.
(36) Demir, P.; Onde, S.; Severcan, F. Phylogeny of cultivated and wild wheat species using ATR-FTIR spectroscopy. *Spectrochimica Acta Part A: Molecular and Biomolecular Spectroscopy* **2015**, *135*, 757−763.
(37) Wold, S.; Esbensen, K.; Geladi, P. Principal component analysis. *Chemometrics and Intelligent Laboratory Systems* **1987**, *2* (1), 37−52.
(38) Asakura, T. Structure of Silk I (Bombyx mori Silk Fibroin before Spinning) -Type II β-Turn, Not α-Helix. *Molecules* **2021**, *26* (12), 3706.
(39) Krimm, S.; Bandekar, J. Vibrational Spectroscopy and Conformation of Peptides, Polypeptides, and Proteins. In *Advances in Protein Chemistry*; Anfinsen, C. B., Edsall, J. T., Richards, F. M., Eds.; Academic Press: 1986; Vol. *38*, pp 181−364.
(40) Jackson, M.; Mantsch, H. H. The Use and Misuse of FTIR Spectroscopy in the Determination of Protein Structure. *Crit. Rev. Biochem. Mol. Biol.* **1995**, *30* (2), 95−120.
(41) Pribic, R.; Vanstokkum, I. H. M.; Chapman, D.; Haris, P. I.; Bloemendal, M. Protein Secondary Structure from Fourier Transform Infrared and/or Circular Dichroism Spectra. *Anal. Biochem.* **1993**, *214* (2), 366−378.
(42) Dousseau, F.; Pezolet, M. Determination of the secondary structure content of proteins in aqueous solutions from their amide I and amide II infrared bands. Comparison between classical and partial least-squares methods. *Biochemistry* **1990**, *29* (37), 8771−8779.
(43) Venyaminov, S. Y.; Kalnin, N. N. Quantitative IR spectrophotometry of peptide compounds in water (H_2O) solutions. I. Spectral parameters of amino acid residue absorption bands. *Biopolymers* **1990**, *30* (13−14), 1243−1257.
(44) De Meutter, J.; Goormaghtigh, E. Amino acid side chain contribution to protein FTIR spectra: impact on secondary structure evaluation. *Eur. Biophys. J.* **2021**, *50* (3), 641−651.
(45) Anderle, G.; Mendelsohn, R. Thermal denaturation of globular proteins. Fourier transform-infrared studies of the amide III spectral region. *Biophys. J.* **1987**, *52* (1), 69−74.
(46) Kaiden, K.; Matsui, T.; Tanaka, S. A Study of the Amide III Band by FT-IR Spectrometry of the Secondary Structure of Albumin, Myoglobin, and γ-Globulin. *Appl. Spectrosc.* **1987**, *41* (2), 180−184.
(47) Cai, S.; Singh, B. R. A Distinct Utility of the Amide III Infrared Band for Secondary Structure Estimation of Aqueous Protein Solutions Using Partial Least Squares Methods. *Biochemistry* **2004**, *43* (9), 2541−2549.
(48) Kalnin, N. N.; Baikalov, I. A.; Venyaminov, S. Y. Quantitative IR spectrophotometry of peptide compounds in water (H_2O)

https://doi.org/10.1021/acsapm.3c01892
ACS Appl. Polym. Mater. 2023, 5, 9433−9444

solutions. III. Estimation of the protein secondary structure. *Biopolymers* **1990**, *30* (13−14), 1273−1280.
(49) Venyaminov, S. Y.; Kalnin, N. N. Quantitative IR spectrophotometry of peptide compounds in water (H_2O) solutions. II. Amide absorption bands of polypeptides and fibrous proteins in α-, β-, and random coil conformations. *Biopolymers* **1990**, *30* (13−14), 1259−1271.
(50) Hassan, M.; Ilev, I. Grazing incidence angle based sensing approach integrated with fiber-optic Fourier transform infrared (FO-FTIR) spectroscopy for remote and label-free detection of medical device contaminations. *Rev. Sci. Instrum.* **2014**, *85* (10), 103108.
(51) Kim, S.; Burgula, Y.; Ojanen-Reuhs, T.; Cousin, M. A.; Reuhs, B. L.; Mauer, L. J. Differentiation of Crude Lipopolysaccharides from Escherichia coli Strains Using Fourier Transform Infrared Spectroscopy and Chemometrics. *J. Food Sci.* **2006**, *71* (2), M57−M61.
(52) Krasnov, I.; Diddens, I.; Hauptmann, N.; Helms, G.; Ogurreck, M.; Seydel, T.; Funari, S. S.; Müller, M. Mechanical Properties of Silk: Interplay of Deformation on Macroscopic and Molecular Length Scales. *Phys. Rev. Lett.* **2008**, *100* (4), 048104.
(53) Papadopoulos, P.; Sölter, J.; Kremer, F. Structure-property relationships in major ampullate spider silk as deduced from polarized FTIR spectroscopy. *Eur. Phys. J. E* **2007**, *24* (2), 193−199.
(54) Ene, R.; Papadopoulos, P.; Kremer, F. Supercontraction in Nephila spider dragline silk - Relaxation into equilibrium state. *Polymer* **2011**, *52* (26), 6056−6060.
(55) Hirschfeld, T. Diagnosis and correction of wedging errors in absorbance subtract Fourier transform infrared spectrometry. *Anal. Chem.* **1979**, *51* (4), 495−499.
(56) Davis, B. J.; Scott Carney, P.; Bhargava, R. Theory of Infrared Microspectroscopy for Intact Fibers. *Anal. Chem.* **2011**, *83* (2), 525−532.
(57) Mayerhöfer, T. G.; Pahlow, S.; Popp, J. The Bouguer-Beer-Lambert Law: Shining Light on the Obscure. *ChemPhysChem* **2020**, *21* (18), 2029−2046.
(58) Averett, L. A.; Griffiths, P. R.; Nishikida, K. Effective Path Length in Attenuated Total Reflection Spectroscopy. *Anal. Chem.* **2008**, *80* (8), 3045−3049.
(59) Boulet-Audet, M.; Buffeteau, T.; Boudreault, S.; Daugey, N.; Pézolet, M. Quantitative Determination of Band Distortions in Diamond Attenuated Total Reflectance Infrared Spectra. *J. Phys. Chem. B* **2010**, *114* (24), 8255−8261.
(60) Corujo, M. P.; Sklepari, M.; Ang, D. L.; Millichip, M.; Reason, A.; Goodchild, S. C.; Wormell, P.; Amarasinghe, D. P.; Lindo, V.; Chmel, N. P.; Rodger, A. Infrared absorbance spectroscopy of aqueous proteins: Comparison of transmission and ATR data collection and analysis for secondary structure fitting. *Chirality* **2018**, *30* (8), 957−965.
(61) Rodger, A.; Steel, M. J.; Goodchild, S. C.; Chmel, N. P.; Reason, A. Transformation of aqueous protein attenuated total reflectance infra-red absorbance spectroscopy to transmission. *QRB Discovery* **2020**, *1*, No. e8.
(62) Arndt, T.; Greco, G.; Schmuck, B.; Bunz, J.; Shilkova, O.; Francis, J.; Pugno, N. M.; Jaudzems, K.; Barth, A.; Johansson, J.; Rising, A. Engineered Spider Silk Proteins for Biomimetic Spinning of Fibers with Toughness Equal to Dragline Silks. *Adv. Funct. Mater.* **2022**, *32* (23), 2200986.
(63) Greco, G.; Arndt, T.; Schmuck, B.; Francis, J.; Bäcklund, F. G.; Shilkova, O.; Barth, A.; Gonska, N.; Seisenbaeva, G.; Kessler, V.; Johansson, J.; Pugno, N. M.; Rising, A. Tyrosine residues mediate supercontraction in biomimetic spider silk. *Commun. Mater.* **2021**, *2* (1), 43.

https://doi.org/10.1021/acsapm.3c01892
ACS Appl. Polym. Mater. 2023, 5, 9433−9444